2017-09-13

Simulation and analysis of wave-structure interactions for a semi-immersed horizontal cylinder

Tan Loh, T

10.1016/j.oceaneng.2017.08.059
Ocean Engineering
Elsevier BV

This paper is published in Ocean Engineering, an International Journal of Research and Development (Elsevier) and can be accessed online at:
http://www.sciencedirect.com/science/article/pii/S0029801817304948

Note* Please cite this article in press as: Tan Loh, T., et al., Simulation and analysis of wave-structure interactions for a semi-immersed horizontal cylinder, Ocean Engineering (2017), http://dx.doi.org/10.1016/j.oceaneng.2017.08.059

Simulation and Analysis of Wave-Structure Interactions for a Semi-Immersed Horizontal Cylinder

[#1]T. Tan Loh, [*2]D. Pizer, [#3]D. Simmonds, [#4]A. Kyte and [#5]D. Greaves

[#]*Plymouth University, School of Marine Science and Engineering, Drakes Circus, Plymouth, PL4 8AA, United Kingdom.*
[1]teng.tanloh@postgrad.plymouth.ac.uk
[3]D.Simmonds@plymouth.ac.uk
[4]adam.kyte@plymouth.ac.uk
[5]deborah.greaves@plymouth.ac.uk

[*]*Independent Consultant, Edinburgh, United Kingdom.*
[2]davidpizer@gmail.com

Abstract

The paper is concerned with the use of the open source computational fluid dynamics software package, OpenFOAM® for predicting and analysing the behaviour of a semi-immersed horizontal cylinder subject to different types of ocean wave conditions. This study involves two separate cases of wave-structure interaction involving a semi-immersed horizontal cylinder, which may represent the simplified form of a cylindrical component of a wave energy converter. First, the flow around a fixed semi-immersed horizontal cylinder subject to regular waves is studied, in which the horizontal and vertical forces are computed and compared to linear wave theory and available experimental data. Further, a semi-immersed horizontal cylinder with a prescribed oscillatory vertical motion is considered to determine the surface wave elevations generated by the motion of the cylinder. The measured numerical surface elevations are also compared with theoretical predictions and experimental data. Both cases considered in this paper are simulated in a numerical wave tank where wave relaxation zones are utilised to avoid wave reflections. It is concluded that the numerical data produced by OpenFOAM® provide good overall agreement within the limitations of the relevant theory and experiment data.

Keywords: Semi-immersed horizontal cylinder, Oscillating horizontal cylinder, OpenFOAM®, Waves2Foam, Numerical wave tank

1. Introduction

The marine renewable energy industry is still at a nascent stage, but is considered a key part of the strategy to hit the targets of renewable energy supply set by the UK government for 2020. Whilst innovative marine renewable energy device technologies have received a great deal of interest in generating clean and sustainable energy, the technicalities of operating them in hostile environments remain complex and challenging. In practice, wave energy converters (WEC) are required to operate efficiently under many different types of wave

conditions and designed to optimally extract energy from ocean waves. To achieve this goal, complex wave-structure interactions involved in WEC operation need to be modelled accurately under a wide range of conditions. Existing theoretical solutions are based on approximations which are often too restrictive to simulate the WEC performance accurately. Linear potential theory is widely used and is valid if the wave amplitude and body motions are not too large compared to the body dimensions, and if the wave steepness is not too great. These methods accurately take into account wave diffraction and radiation effects, but neglect viscous effects and non-linear effects. For smaller bodies in larger and steeper waves, empirical methods (e.g. the MOJS equation by Morison, O'Brien, Johnson and Schaaf, 1950) are more appropriate as they can incorporate non-linear and viscous effects, but they may not accurately model wave diffraction and radiation effects. Computational fluid dynamics (CFD) methods are capable of incorporating all non-linear wave diffraction, radiation and viscous effects and can therefore provide a solution which is valid over a wide range of wave and body motion regimes.

The main aim of this study is to gain a better understanding of the hydrodynamic analysis of wave-structure interactions for a semi-immersed horizontal cylinder when operating under different types of wave conditions. This study also serves as a foundation to provide the fundamental knowledge of the interactions of a cylindrical attenuator type WEC with ocean waves. The simulations in this study are carried out using OpenFOAM®, an open source CFD software package, which uses the finite volume method for solving the discretised Navier-Stokes equations. Two separate cases of a semi-immersed horizontal cylinder are considered, which may represent the simplified form of a cylindrical component of a WEC. The first case is carried out to model the structure as a fixed obstacle, in the form of a semi-immersed horizontal cylinder, which is placed in the numerical wave tank (NWT) and subject to an incident wave at one end of the tank. The wave induced vertical and horizontal forces (lift and drag) acting on the cylinder are then computed from the pressure and the shear stress data. In the second case, the structure is floating and consideration is given to a semi-immersed horizontal cylinder subject to a forced sinusoidal vertical displacement. The resulting surface wave elevations generated by the structure are then computed for various structure oscillation amplitudes and frequencies. Results for both cases are compared with existing theories which are valid under certain simplified assumptions. Available experimental data in the literature are also compared with the numerical results. Both cases are simulated in a two-dimensional (2D) NWT using waves2Foam, a third party toolbox developed by Jacobson et al. (2012) within OpenFOAM® for wave generations and wave absorptions.

Various authors have considered wave interaction with a fixed semi-immersed horizontal cylinder, such as Dean and Ursell (1959), Dixon et al. (1979), Dixon (1980), Martin and Dixon (1983), Andersson (2011), Westphalen et al. (2012), Bihs et al. (2013), Chen et al. (2015) and Ong et al. (2017). Martin and Dixon (1983) carried out a linear wave theory prediction for the forces acting on a fixed cylinder. They also generated experimental data for various wave frequencies and medium wave amplitudes for comparison with linear wave theory. Martin and Dixon (1983) used classical potential theory, in which the two

dimensional diffraction boundary-value problems are solved linearly using Ursell's multipole method. Dean and Ursell (1959) also carried out experiments for measuring the forces acting on a fixed horizontal cylinder for various wave frequencies but under low wave amplitude conditions. Dixon et al. (1979) and Dixon (1980) used an equation based on Morison et al. (1950) to predict the vertical wave forces acting on partially submerged cylinders for comparing the theoretical predictions with the experimental results conducted as part of the Edinburgh Wave Power Project. Westphalen et al. (2012) reproduced some of the experimental data by Dixon et al. (1979) on a fixed horizontal cylinder using STAR-CCM+® and ANSYS CFX®. Andersson (2011) carried out similar numerical investigation using OpenFOAM® and compared his numerical results with Westphalen et al. (2012). Both Westphalen et al. (2012) and Andersson (2011) only simulated a single wave frequency and wave height for each of the three different cylinder submergence depths. They mainly concentrated on the large amplitude waves in order to establish the non-linear behaviour of the vertical forces acting on the cylinder. This paper examines the gradual transition of the linear to non-linear behaviour of the horizontal and the vertical forces on the cylinder when subject to waves with different wave heights and wave frequencies. Bihs and Ong (2013) carried out 2D numerical simulations using CFD model to investigate free surface waves past a single semi-submerged cylinder, whilst Ong et al. (2017) carried out similar study on both single and two semi-submerged horizontal cylinders under turbulent flow. Both studies focused on the vertical forces induced on the cylinder(s), in which the results are compared with experimental data by Dixon et al. (1979). Chen et al. (2015) also investigated wave forces on partially submerged fixed circular and squared cross sections cylinders in a wave tank numerically based on the Navier-Stokes equation. Chen et al. (2015) compared their numerical results with a modified Morison equation (Dixon, 1980) and suggested that the equation tend to underestimate the wave forces. The wave properties and water depth chosen by Chen et al. (2015) are all outside of the range selected in this paper.

Many studies were carried out on an oscillating cylinder in free surface flow by Tasai (1960, 1961), Frank (1967), Vugts (1968), Ramos and Guedes Soares (1997) and Gadelho et al. (2014), they are mainly concentrated on determining the hydrodynamic coefficients and the forces of the oscillating cylinder. Recently, Gadelho et al. (2014) presented a study on determining the hydrodynamic coefficients of an oscillating 2D cylinder using OpenFOAM® and compared the results for heave and sway motions of the cylinder in deep water with the experimental data by Sutulo et al. (2009, 2010). Whilst Chung (2015) investigated the effects of the oscillating cylinder motion on the free surface deformations, the cylinder was fully submerged beneath the free surface. The second case in this paper is based on a study by Yu and Ursell (1961) and Ursell (1949), where a potential flow theory is used to predict surface wave amplitudes that are generated when a semi-immersed horizontal cylinder is subject to a small forced oscillation in the vertical direction. The theory is valid for finite water depths and results were generated for a wide range of wave frequencies. Yu and Ursell (1961) also generated experimental wave amplitude data in a physical tank which were compared with their linear wave theory predictions.

Section 2 of this paper provides a description of the methodology and the theoretical analysis for this study. It describes the governing equations leading to the Navier-Stokes equations solved within OpenFOAM® and the definition of the NWT. The features of the wave generation toolbox, waves2foam are explained to show how waves generated in a physical wave tank can be replicated in a NWT. Section 2 describes the theoretical analysis of the wave induced forces on a semi-immersed horizontal cylinder using a linearized wave theory by Martin and Dixon (1983). Comparisons are also made with a non-linear theory provided by Dixon et al. (1979) and Dixon (1980) which uses an empirical formula, based on Morison et al. (1950), to predict the horizontal and the vertical wave forces. Section 2 also shows a brief summary of the theory developed by Yu and Ursell (1961) for predicting surface waves generated by an oscillating cylinder. Section 3 of this paper focuses on the application of the numerical method discussed in Section 2 in order to simulate the fixed cylinder and the oscillating cylinder cases. The numerical results are analysed and compared with both the theoretical predictions and experimental data from the literature. The numerical results presented in Section 3 also show the transition of the wave forces and surface wave amplitude ratios of the cylinder in more detail towards non-linearity and divergence from linear theory, as well as the validity and limitation of the linear theory. Section 4 is devoted to the overall conclusions of the work carried out in this paper.

2. Theoretical Analysis

2.1 Governing equations for fluid flow

This study was carried out using OpenFOAM® (Open Field Operation And Manipulation), an open source CFD software package comprised of C++ libraries and codes developed by OpenCFD Ltd at ESI Group . OpenFOAM® consists of a wide range of features and capabilities for solving continuum mechanics such as chemical reactions, turbulence, heat transfer, solid dynamics and electromagnetics (Greenshields, 2015). The solvers used in this study are interFoam and interDyMFoam. Both solvers are designed for multiphase flows which uses a VOF (volume of fluid) phase-fraction based interface for solving two incompressible, isothermal immiscible fluids. Whilst interDyMFoam is designed for similar applications as in interFoam, it has the option of mesh motion and mesh topology changes. Both solvers use a finite volume method for discretizing the Navier-Stokes equations, in which the fluid flow domain is discretized by creating a grid mesh over the entire domain of interest. In a Cartesian coordinate system (x,y,z), the governing equation of motion for a time-dependent three-dimensional multiphase (air and water) incompressible laminar fluid is described as

$$\frac{\partial \rho \mathbf{u}}{\partial t} + \nabla \cdot \left[\rho \mathbf{u}\mathbf{u}^T\right] = -\nabla p^* + \nabla \cdot \left[\mu \nabla \mathbf{u}\right] + \sigma_T \kappa_\gamma \nabla \gamma \ , \tag{1}$$

where t is the time, ∇ is a vector differential operator, $\mathbf{u}$, $\mathbf{u}^T$ is the velocity vector and velocity vector transpose respectively of a fluid element, p^* is the gauge pressure, μ is the dynamic viscosity of the multiphase fluid, ρ is the density of the multiphase fluid, σ_T is the surface

tension coefficient, κ_γ is the surface curvature of the air-water interface, γ $(0 \le \gamma \le 1)$ is the water volume fraction in a mesh cell ($\gamma = 0$ for air only and $\gamma = 1$ for water only). Coupled with the equation of motion (1), for incompressible flows, the equation of continuity can be written as

$$\nabla \cdot \mathbf{u} = 0 . \tag{2}$$

In OpenFOAM®, the VOF method by Hirt et al. (1981), is used to track the water volume fraction quantity, γ which is modelled by the modified advection equation

$$\frac{\partial \gamma}{\partial t} + \nabla \cdot [\mathbf{u}\gamma] + \nabla \cdot [\mathbf{u}_{\mathrm{r}} \gamma(1-\gamma)] = 0 , \tag{3}$$

where $\mathbf{u}_{\mathrm{r}}$ is a relative velocity. The modified advection equation (3) has an additional term $\nabla \cdot [\mathbf{u}_{\mathrm{r}} \gamma(1-\gamma)]$ which is used to limit the amount of interface smearing. The solution for γ in equation (3) is used to calculate the density and dynamic viscosity of the multiphase fluid used in equation (1). These quantities are obtained from the equations,

$$\rho = \gamma \rho_{\mathrm{water}} + (1-\gamma)\rho_{\mathrm{air}} \qquad \text{and} \qquad \mu = \gamma \mu_{\mathrm{water}} + (1-\gamma)\mu_{\mathrm{air}} , \tag{4}$$

where ρ_{water} and ρ_{air} are the densities of water and air respectively and μ_{water} and μ_{air} are the dynamic viscosities of water and air respectively. The pressure-velocity equation (1) is solved using the PISO (Pressure Implicit with Splitting of Operators) algorithm in conjunction with the VOF method for calculating the water volume fraction in equation (3).

2.2 Numerical wave tank (NWT)

The physical characteristics of a physical wave tank in the laboratory can be replicated closely by a NWT. In order to achieve this, the boundary conditions of the NWT must be defined to imitate the behaviour of the physical wave tank when generating wave motion. Waves2Foam, a third party toolbox developed by Jacobson et al. (2012) in OpenFOAM® is utilised in this study for both wave generation and absorption. Wave relaxation zones are implemented to prevent reflection of waves from outlet boundaries and waves reflected internally in the computational domain which can interfere with the wave maker boundaries. In order to satisfy certain continuity conditions at the relaxation zone boundaries, Jacobsen et al. (2012) extended Mayer et al. (1998) relaxation technique, in which the relaxation function is given by

$$\mathbf{u} = \alpha_R \mathbf{u}_{\mathrm{computed}} + (1-\alpha_R)\mathbf{u}_{\mathrm{target}} \qquad \text{and} \qquad \gamma = \alpha_R \gamma_{\mathrm{computed}} + (1-\alpha_R)\gamma_{\mathrm{target}} , \tag{5}$$

$$\text{with} \qquad \alpha_R(\chi_R) = 1 - \frac{\exp(\chi_R^{3.5}) - 1}{\exp(1) - 1} \qquad \text{for} \quad \chi_R \in [0;1], \tag{6}$$

where the variation of α_R is the same as given by Fuhrman et al. (2006). χ_R is a scaled distance over the relaxation region. $\chi_R = 0$ corresponds to the interface between the relaxed and non-relaxed region in the NWT and $\chi_R = 1$ corresponds to the end walls of the NWT. $\mathbf{u}_{\text{computed}}$ and $\mathbf{u}_{\text{target}}$ are the numerically computed velocity and target velocity respectively evaluated at point χ_R in the relaxation zone and γ_{computed}, γ_{target} are the numerically computed volume fraction and target volume fraction respectively at point χ_R in the relaxation zone. The target velocity, $\mathbf{u}_{\text{target}}$ is based on inlet wall theory being extended over the inlet relaxation zone but has a zero value in the outlet relaxation zone. The target volume fraction, γ_{target} is based on the imposed inlet wave field being extended over the inlet relaxation zone whilst in the outlet relaxation zone, the target volume fraction is based on still water elevation as illustrated in Fig. 1.

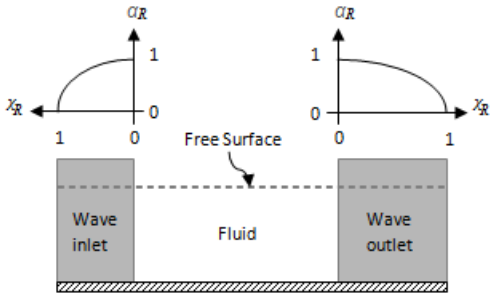

Fig. 1: The relaxation zone at both inlet and outlet (Jacobson et al., 2012).

There are multiple wave theories available within the toolbox for generating different types of waves in the NWT, for instance 1st, 2nd and 5th order Stokes waves, solitary waves, cnoidal waves, stream function waves and irregular waves. Based on the validity of several theories for periodic water waves in Le Méhauté (1976), Stokes second order wave theory is best suited for the wave parameters selected in this study. The relevant second order Stokes wave theory quantities for free surface elevation and wave velocity components are defined at the inlet boundary of the NWT and presented as follows. The free surface elevation, η, for a Stokes second order wave is described by the formula

$$\eta = \frac{H}{2}\cos(\omega t - kx) + \left(\frac{H^2 k}{16}\right)\frac{\cosh(kh)}{\sinh^3(kh)}\left[2 + \cosh(2kh)\right]\cos\left[2(\omega t - kx)\right], \tag{7}$$

where H is the wave height, h is the water depth, ω is the wave frequency, k is the wave number, t is the time and x is the left to right Cartesian coordinate which coincides with the mean height of the wave. The incident waves are generated by applying the u, horizontal and v, vertical particle velocity components on the inlet boundary based on the Stokes second order wave theory, and are given by

$$u = \frac{\omega H}{2}\frac{\cosh\left[k(y+h)\right]}{\sinh(kh)}\cos(\omega t - kx) + \frac{3}{16}\left(\frac{\omega}{k}\right)(kH)^2\frac{\cosh\left[2k(y+h)\right]}{\sinh^4(kh)}\cos\left[2(\omega t - kx)\right] - U, \tag{8}$$

$$v = -\frac{\omega H}{2}\frac{\sinh[k(y+h)]}{\sinh(kh)}\sin(\omega t - kx) - \frac{3}{16}\left(\frac{\omega}{k}\right)(kH)^2\frac{\sinh[2k(y+h)]}{\sinh^4(kh)}\sin[2(\omega t - kx)], \qquad (9)$$

where y is the Cartesian coordinate in the upward vertical direction with $y = 0$ being the still water level , $U = \frac{gkH^2}{8\omega h}$ is the mean velocity in the x direction on the inlet boundary, g is a gravitational acceleration. Subtraction of the U term in equation (8) ensures a zero mean velocity for u on the inlet boundary.

2.3 Forces induced on a fixed semi-immersed horizontal cylinder based on linear wave theory

This section contains a brief summary of the theory developed by Martin and Dixon (1983) for predicting the scattering of regular surface waves, by a fixed semi-immersed horizontal cylinder, in an infinite depth of water. The theory is only valid for small amplitude waves. Fig. 2 shows a half-immersed circular cylinder in an infinite expanse of water. A regular wave is generated towards the cylinder which causes a reflected wave and a transmitted wave to occur which moves away from the cylinder.

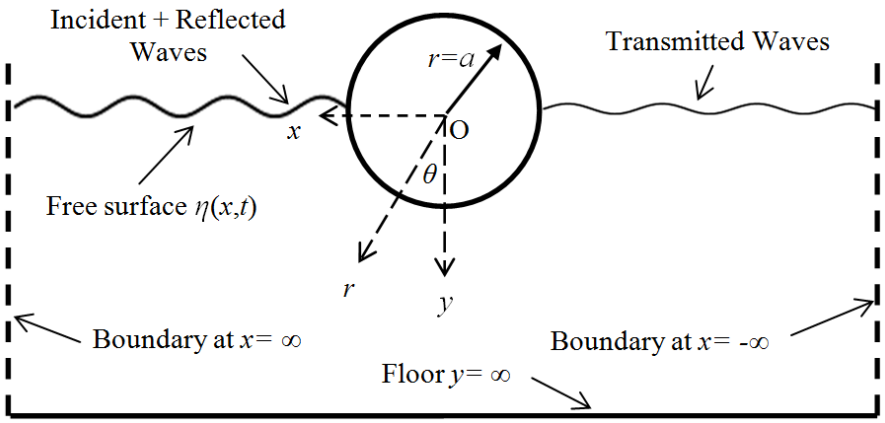

Fig. 2: A fixed semi-immersed horizontal cylinder subject to an incident wave.

As shown in Fig. 2, a Cartesian coordinate system is used where the origin is at the centre of the cylinder of radius a, the x axis is the right to left horizontal direction and points towards the incident wave, and the y axis is in the downward vertical direction with $y = 0$ being the still water level. It should be noted that the (x,y) directions in Fig. 2 have been defined to be in the opposite directions to those used in the linear wave theory in Section 2.2.

Let r and θ be polar coordinates which are related to the Cartesian coordinates by the equations

$$x = r\sin(\theta) \quad \text{and} \quad y = r\cos(\theta), \quad r > a, \quad -\frac{\pi}{2} < \theta < \frac{\pi}{2}. \qquad (10)$$

The inviscid velocity flow potential $\phi(x,y,t)$ in the fluid satisfies the Laplace equation

$$\left(\frac{\partial^2}{\partial x^2}+\frac{\partial^2}{\partial y^2}\right)\phi(x,y,t)=0 \qquad -\infty<x<\infty,\quad 0<y<\infty,\quad r>a\,, \tag{11}$$

subject to the linearised boundary condition

$$K\phi+\frac{\partial\phi}{\partial y}=0 \text{ on the free surface } y=0,\quad r>a\,, \text{ where } K=\frac{\omega^2}{g}. \tag{12}$$

The potential function must satisfy the normal velocity condition on the cylinder given by

$$\frac{\partial\phi}{\partial r}=0 \text{ on } r=a,\ -\frac{\pi}{2}<\theta<\frac{\pi}{2}. \tag{13}$$

The potential function $\phi(x,y,t)$ is assumed to be harmonic in time which can be written in the complex form

$$\phi(x,y,t)=\mathrm{Re}\left[\phi(x,y)e^{-j\omega t}\right]\,, \tag{14}$$

where ω is the wave frequency, t is time, j is a unit imaginary number and Re denotes the real part of a complex expression. The free surface coefficient of the incident wave is assumed to be of the form

$$\eta(x,t)=-jAe^{-jKx},\ |x|>a\,, \tag{15}$$

where A is a complex wave amplitude. The incident wave will cause a reflected wave and transmitted wave on the cylinder. In which case the free surface coefficient on both sides of the cylinder may be expressed as

$$\eta(x,t)=\begin{cases}-jA\left[e^{-jKx}+Re^{jKx}\right], & x>a\\ -jATe^{-jKx}, & x<-a\end{cases}\,, \tag{16}$$

where R is a reflection coefficient and T is a transmission coefficient. Due to energy conservation, the reflection and transmission coefficients must satisfy the equation

$$|R|^2+|T|^2=1. \tag{17}$$

Of particular interest in this study is the calculation of the horizontal force, F_x, and the vertical force, F_y, acting on the cylinder which can be shown to be given by the formulae

$$F_x=-ja\omega\rho\int_{-\pi/2}^{\pi/2}\phi|_{r=a}\sin(\theta)d\theta,\ F_y=-ja\omega\rho\int_{-\pi/2}^{\pi/2}\phi|_{r=a}\cos(\theta)d\theta\,, \tag{18}$$

where ρ is the water density. To solve equations (11)-(13), Martin and Dixon (1983) expressed the potential function in terms of an infinite series of multipole functions (Thorne, 1953), containing undetermined coefficients, which automatically satisfied equations (11) and (12). To satisfy equation (13), the coefficients of the series were chosen to give a good approximate fit to equation (13). This approximation involved a procedure which is similar to a Fourier series approximation to a function over the range $-\frac{\pi}{2} < \theta < \frac{\pi}{2}$.

2.4 Forces induced on a fixed semi-immersed horizontal cylinder based on Morison equation

The theory discussed in Section 2.3 is only valid for small amplitude waves. In order to compare the simulation results for larger amplitude waves, a Morison empirical formula was used. Morison et al. (1950) proposed an empirical formula for calculating the horizontal wave force, F_h, acting on a vertical cylindrical column given by

$$F_h = C_m \rho V \frac{\partial U_h}{\partial t} + \frac{1}{2} C_D \rho S |U_h| U_h, \tag{19}$$

where ρ is the water density, S is the projected area of column per unit length normal to the wave plane, U_h is the horizontal component of the water velocity, V is the volume per unit length of the column, C_m is the coefficient of inertia and C_D is the drag coefficient.

Borgman (1958) and Chakrabarti et al. (1975) show that equation (19) should be slightly modified, for horizontal or inclined cylinders, to the formula for the horizontal or vertical force, $F_{h,v}$, given by

$$F_{h,v} = C_m \rho V \frac{\partial U_{h,v}}{\partial t} + \frac{1}{2} C_D \rho S |W| U_{h,v}, \tag{20}$$

where $U_{h,v}$ is the horizontal or vertical component of the water velocity and W is the normal fluid particle velocity.

However equation (20) only apply to cylinders which are completely immersed in water. Dixon et al (1979) proposed a modification to equation (20) for semi-immersed horizontal cylinders which takes into account the buoyancy of the cylinder to give the vertical force component

$$F_v = C_m \rho V \frac{\partial U_v}{\partial t} + \rho g [V(t) - V_0], \tag{21}$$

where g is the gravitational acceleration, V_0 is the initial immersed volume (in the absence of waves) and $V(t)$ is the immersed volume of the cylinder in the presence of a wave as a function of time t. It should be noted that Dixon et al. (1979) ignored the drag term in

equation (21) since it was shown by Garrison and Rao (1971) that this term is small when the cylinder diameter is large compared with the wave amplitude.

Dixon et al. (1979) and Dixon (1980) used equation (21) to derive an approximate formula for the vertical force of a partially submerged horizontal cylinder in deep water in which the centre of the cylinder is at any position above or below the still water line. In the special case when the centre of the cylinder is at the still water line, their formula reduced to

$$F_v = -C_m \frac{\pi g \rho l D^2}{4L} \eta(t) \left[\pi + \frac{4\eta(t)}{D} \sqrt{1 - \frac{4\eta(t)^2}{D^2}} + 2\sin^{-1}\left(\frac{2\eta(t)}{D} \right) \right] + \frac{\rho g l D^2}{8} \left[\frac{4\eta(t)}{D} \sqrt{1 - \frac{4\eta(t)^2}{D^2}} + 2\sin^{-1}\left(\frac{2\eta(t)}{D} \right) \right]. \quad (22)$$

where D is the cylinder diameter, A is the wave amplitude, T is the wave period, L is the wavelength, l is the cylinder length and $\eta(t) = A\sin\left(\frac{2\pi t}{T}\right)$ is the surface wave equation. In the derivation of equation (22), Dixon et al. (1979) made the simplifying assumptions that the wave height is small compared with the wavelength (small wave steepness) and the water depth is large compared with the wavelength (deep water). For small wave steepness, buoyancy has a negligible effect in the horizontal direction and on ignoring the drag term, the horizontal force component in equation (20), for deep water, simplifies to (Dixon, 1980)

$$F_h = -C_m \frac{\pi g \rho l D^2 A}{4L} \left[\pi + \frac{4\eta(t)}{D} \sqrt{1 - \frac{4\eta(t)^2}{D^2}} + 2\sin^{-1}\left(\frac{2\eta(t)}{D} \right) \right] \cos\left(\frac{2\pi t}{T} \right). \quad (23)$$

2.5 Surface waves generated by a vertically oscillating horizontal cylinder

The theory behind the Yu and Ursell (1961) paper is based on potential flow theory, where the fluid is inviscid and of uniform density. Non-linear terms in the equations of motion are ignored. The motion is assumed to be two-dimensional and the wave channel is of infinite length in the left and right horizontal direction normal to the axis of the cylinder. The Yu and Ursell (1961) theory described in this section is valid for a finite water depth. These authors computed wave amplitudes, at an infinite distance away from the cylinder, for ratios h/a = 2, 4, 10 and ∞ where h is the water depth and a is the radius of the cylinder. The fundamental theory is based on a horizontal semi-submerged horizontal circular cylinder forced to perform small amplitude sinusoidal motion in the vertical direction as shown in Fig. 3.

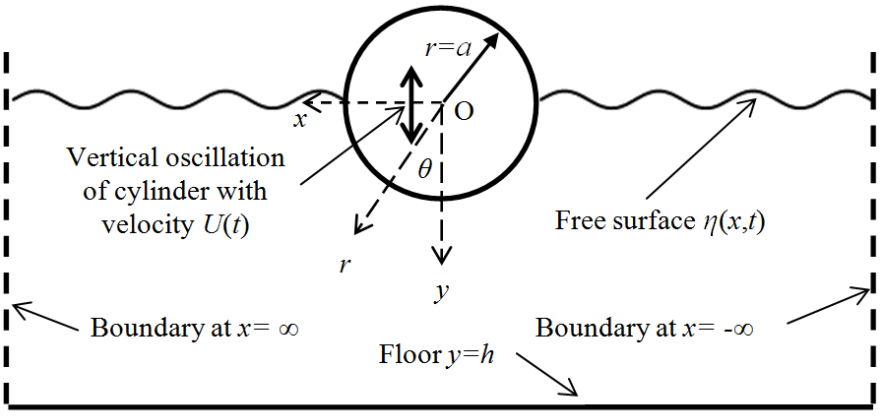

Fig. 3: Horizontal cylinder under forced sinusoidal vertical displacement.

In this section, the Cartesian and polar coordinate system is chosen to be in the same directions as those defined in Section 2.3 and are related to each other by equation (10).

Let the sinusoidal vertical velocity of the cylinder be $V(t)$ oscillating at a frequency, ω, where t is the time. It should be noted that the oscillating frequency, ω, will have the same value as the generated wave frequency.

The Laplace equation, equation (11), and the linearised boundary condition shown in equation (12) are valid for the forced sinusoidal vertical displacement problem considered in this section.

The finite depth condition requires the normal velocity on the ocean floor $y=h$ to be zero in which case the potential function satisfies the condition

$$\frac{\partial \phi}{\partial y} = 0 \text{ on the ocean floor } y = h . \tag{24}$$

The potential function must also satisfy the normal velocity condition on the cylinder wall given by

$$\frac{\partial \phi}{\partial r} = V(t)\cos(\theta) \text{ on } r = a . \tag{25}$$

Additionally, at an infinite distance away from the cylinder, the potential flow field has to satisfy the radiation condition that the waves travel in the outward direction. The free surface $\eta(x,t)$ and pressure distribution $p(x,y,t)$ are related to the potential function by

$$\eta(x,t) = \frac{1}{g}\frac{\partial}{\partial t}\phi(x,0,t) \text{ and } p(x,y,t) = \rho g y - \rho \frac{\partial}{\partial t}\phi(x,y,t). \tag{26}$$

The method for deriving the relationship between the applied cylinder displacement amplitude and the generated ocean wave amplitude follows the work carried out by Yu and Ursell (1969). Parts of the Yu and Ursell (1969) theory follows on from earlier work carried out by Thorne (1953) on multipole expansions.

3. Applications and Validations

3.1 Computational domain setup for a fixed semi-immersed horizontal cylinder

The simulations of a fixed semi-immersed horizontal cylinder are set up in a 16 m long 2D NWT and a water depth of 0.6 m as shown in Fig 4. The semi-immersed horizontal cylinder has a radius, *a* of 0.05 m and length, *l* of 0.295 m. The origin of the cylinder is located at the still water level in the NWT. The second order Stokes wave theory is imposed at the inlet boundary condition as discussed in Section 2.2. A no-slip boundary condition is applied at the tank bed floor, cylinder wall and on the outlet boundary. The top horizontal boundary is set to allow air to enter and leave the domain freely. An inlet relaxation zone of 3.5 m length is located next to the inlet boundary to maintain the characteristic of the incident waves through an imposed wave field at each time step and to prevent internal wave reflections (Jacobsen et al., 2012). An outlet relaxation zone of 7 m with a target solution of still water is located just before the outlet boundary to absorb the transmitted waves. The inlet relaxation zone is chosen to be approximately one incident wavelength and the outlet relaxation zone is chosen to be approximately twice the incident wavelength (largest incident wave length case). The water density is set at 1000 kgm^{-3} with kinematic viscosity of 10^{-6} m^2s^{-1}. The air is set to a density of 1 kgm^{-3} and a kinematic viscosity of 1.48×10^{-5} m^2s^{-1}. No turbulence model is considered in this paper. An Implicit Euler method is used for the time scheme and an automatic time step adjustment function is utilized within OpenFOAM® during the simulation in order to satisfy the Courant-Friedrichs-Lewy (CFL) condition at a maximum value of 0.5.

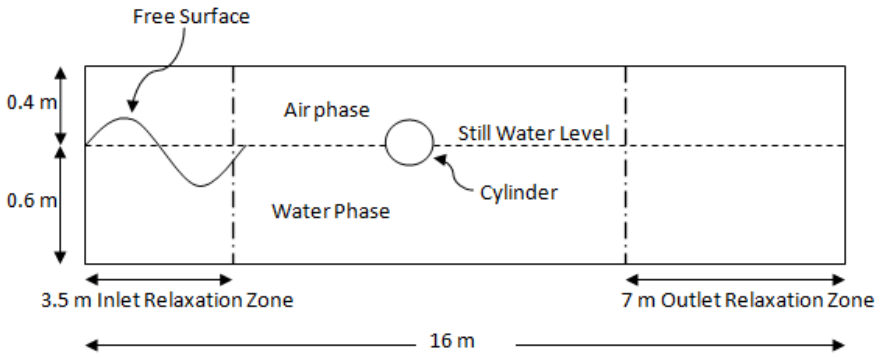

Fig. 4: Schematic of the computational domain setup for the semi-immersed horizontal cylinder in the NWT (not drawn to scale).

An unstructured mesh for the domain is constructed for all the simulations using meshing tools such as blockMesh and snappyHexMesh within OpenFOAM®. In Fig. 5, the mesh is refined in the domain straddling the free surface area to capture accurately the surface elevation and also refined around the cylinder where high velocity gradients are likely to occur. Mesh convergence tests are carried out based on the arrangements presented in Table 1 on the first series of test cases (1 -6) in Table 2 to ensure the solution is independent of grid size.

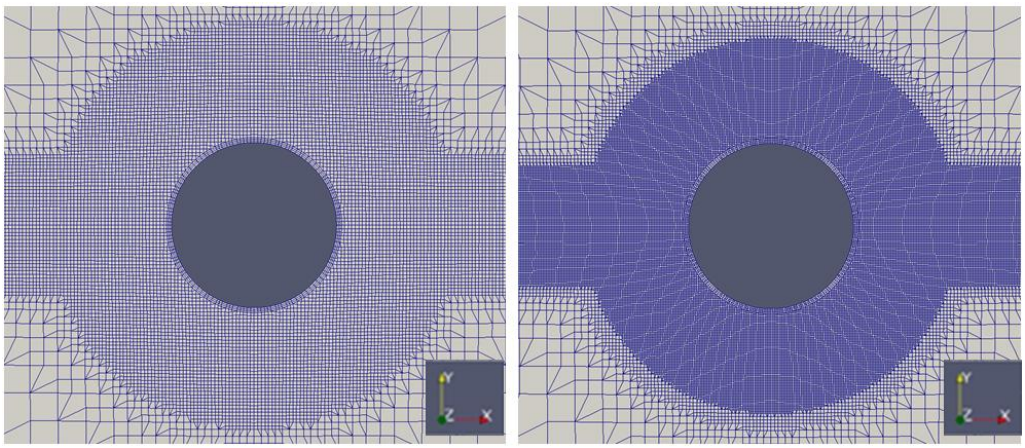

Fig. 5: Close up of the coarse mesh (left) and fine mesh (right) around the cylinder.

Table 1: Mesh refinements for the first series of test cases (1-6) in Table 2.

Mesh Type	**No. of Mesh Elements for Entire Domain**	**Mesh Resolution Closest to Free Surface and Cylinder**
Coarse	Hexahedra: 461,252 Prisms: 56 Polyhedral: 14,416 Total: 475,724	0.2 cm x 0.2 cm
Fine	Hexahedra: 905,672 Prisms: 112 Polyhedral: 29,788 Total: 935,572	0.1 cm x 0.1 cm

Two separate series of test cases are carried out to generate the horizontal forces F_x and the vertical forces F_y on the cylinder. In Table 2, the first series of test cases (1 - 6) are subject to incident waves of various amplitudes with a constant frequency of 1 Hz and a wavelength of 1.539 m. In Table 3, the second series of test cases (7 - 11) are subject to incident waves of different frequencies and wavelengths with constant wave amplitude of 0.02 m.

Table 2: Parameters for the wave components for the first series of test cases (Constants: Frequency, ω = 1.0 Hz, Wavelength, L = 1.539 m).

Test Case	**Wave Amplitude, *A* (m)**	***A/a* (*a*, radius of cylinder)**	**Relative Amplitude, *A′ =(A/D)***
1	0.010	0.2	0.10
2	0.015	0.3	0.15
3	0.020	0.4	0.20
4	0.030	0.6	0.30
5	0.040	0.8	0.40
6	0.050	1.0	0.50

Table 3: Parameters for the wave components for the second series of test cases (Constants: A/a = 0.4, Wave amplitude, A = 0.02 m).

Test Case	Frequency, (Hz)	Wavelength, L (m)	ka
7	0.6	3.458	0.0908
8	0.8	2.270	0.1384
9	1.0	1.539	0.2041
10	1.2	1.081	0.2903
11	1.4	0.796	0.3942

3.2 Validations for forces with linear wave theory and experimental data

A function object in OpenFOAM® is used to calculate the forces and moments by integrating the pressure and skin-friction forces over the patch of the cylinder (Greenshields, 2015). In order to compare the computed horizontal forces F_x and vertical forces F_y with the theoretical and the experiment results by Martin and Dixon (1983), the root-mean-square force F_{RMS} for both of the forces is determined by the formula

$$F_{RMS} = \sqrt{\frac{1}{T}\int_{t=0}^{t=T} f(t)^2 dt} \ , \tag{27}$$

where f (t) is the horizontal or vertical force as a function of time t. The amplitude of the numerical force $F_{x,y}$ is calculated from the root-mean-square force F_{RMS} using the formula

$$F_{x,y} = \sqrt{2} \times F_{RMS} \ . \tag{28}$$

For comparison purposes, the dimensionless quantities of the numerical force amplitude $F_{x,y}'$ is obtained by

$$F_{x,y}' = \frac{F_{x,y}}{\rho g a A l} \ , \tag{29}$$

where ρ is the water density, g is a gravitational acceleration, a is the cylinder radius, A is the incident wave amplitude and l is the length of the cylinder.

Fig. 6(a) shows the comparison of normalised F_x' and F_y' forces calculated using equation (29), simulated in the mesh types based on Table 2 for test cases (1 - 6). Very little discrepancy can be seen between the course and fine mesh indicates that the solution has converged. Fig. 6(b) shows reasonably good agreement between the theoretical predictions, experimental data and the numerical results for the first series of test cases (1 - 6). The discrepancy between the theoretical predictions and the numerical results for the normalised horizontal forces F_x' and the vertical forces F_y' increases with increasing values of A/a. A similar trend of discrepancy also occurs between the theoretical predictions and the

experimental data. The discrepancy for large values of *A/a* is likely to be due to non-linear effects since the linear theory is only valid for small values of *A/a*. According to Martin and Dixon (1983), the linear theory provides a good prediction for their experimental horizontal forces F_x' but has a less accurate prediction for their experimental vertical forces F_y' when *A/a* is small, as shown in Fig. 6(b). In OpenFOAM®, the numerical F_y' and theoretical F_y' forces differ by approximately 4% when *A*/a =0.6 and differ by approximately 1% when *A/a* = 0.4 and 0.2. The numerical F_x' and theoretical F_x' differ by approximately 6% when *A/a* =0.4, by 5% when *A/a* = 0.3 and by 2% when *A/a* = 0.2. Numerical results show better overall agreement with theory than with experimental data at low values of *A/a* ($\leq$ 0.4). For large values of *A/a* (> 0.4), the numerical results for both horizontal and vertical forces show a similar trend to experimental data.

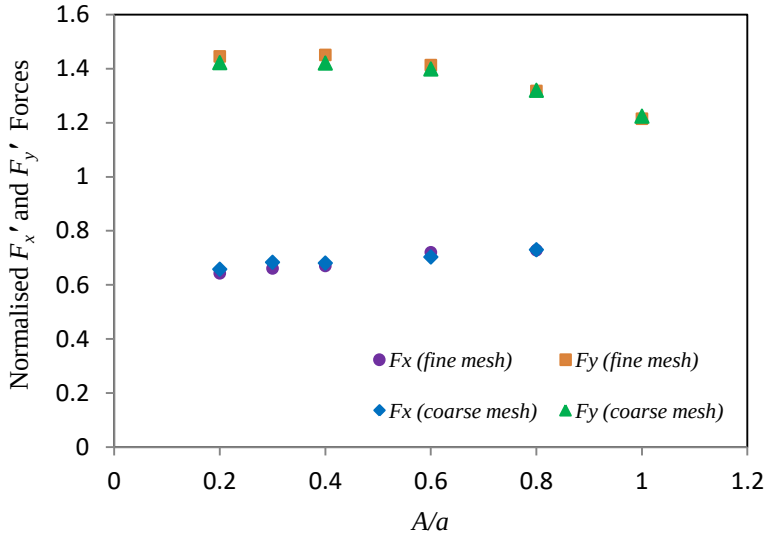

Fig. 6(a): Comparison of normalised F_x' and F_y' forces between coarse and fine meshes for test cases (1 - 6) in terms of *A/a*.

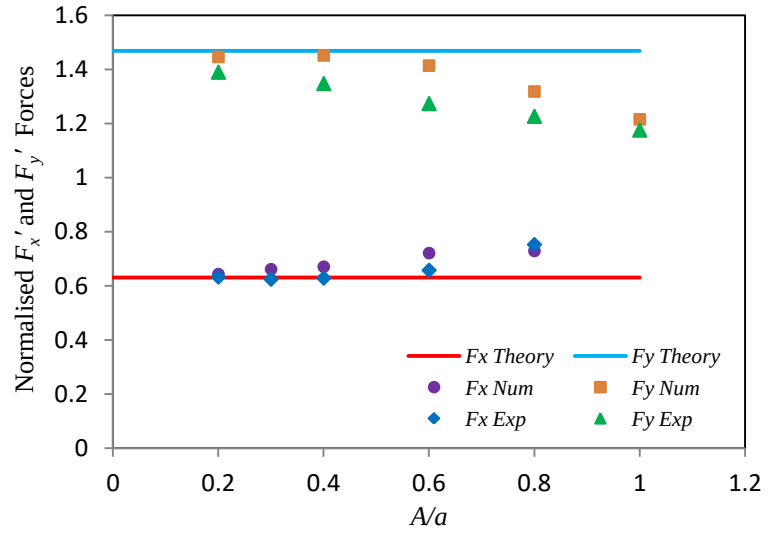

Fig. 6(b): Comparison of normalised F_x' and F_y' forces between numerical result, potential theory and experimental data by Martin and Dixon (1983) for test cases (1 - 6) in terms of *A/a*.

Fig. 7(a) and 7(b) show the comparison between the theoretical predictions, experimental data and numerical results for the second series of test cases (7 - 11) in Table 3 for F_x' and F_y' respectively. Based on these figures, the discrepancy between the theoretical prediction and the experimental data by Martin and Dixon (1983) using A/a = 0.4 for both of the forces, F_x' and F_y', increase as ka increases. Although not presented in this paper, the experimental data by Dean and Ursell (1959) showed good agreement with theory. As pointed out by Martin and Dixon (1983), Dean and Ursell (1959) results were expected to give better agreement with theory since they used smaller values of A/a (< 0.18). Martin and Dixon (1983) suggested that the discrepancy in their own experimental data was likely due to the large value of A/a (0.4) used as previously seen in the first series of test cases in Fig. 6(b). However, in OpenFOAM®, both the numerical horizontal force F_x' and vertical force F_y' appear to be closer to the theoretical predictions than the experiment. The discrepancy between the theoretical prediction and the numerical result for both of the forces, F_x' and F_y' is smaller when compared to Martin and Dixon (1983) experimental data especially when ka increases. It is possible that discrepancies between the numerical results and experimental data are due to the differences in the wave generation and wave absorption methods used in the NWT and the physical wave tank. According to Martin and Dixon (1983), the reflections from the beach in the experiment were up to 5%, whereas the wave relaxation zones in the NWT have been shown to fully absorb the incoming waves (with no change in amplitude at the time that reflected waves would be expected to arrive). However, surface wave elevation data are not available from the experiments and so it is not possible to compare the wave prediction in detail.

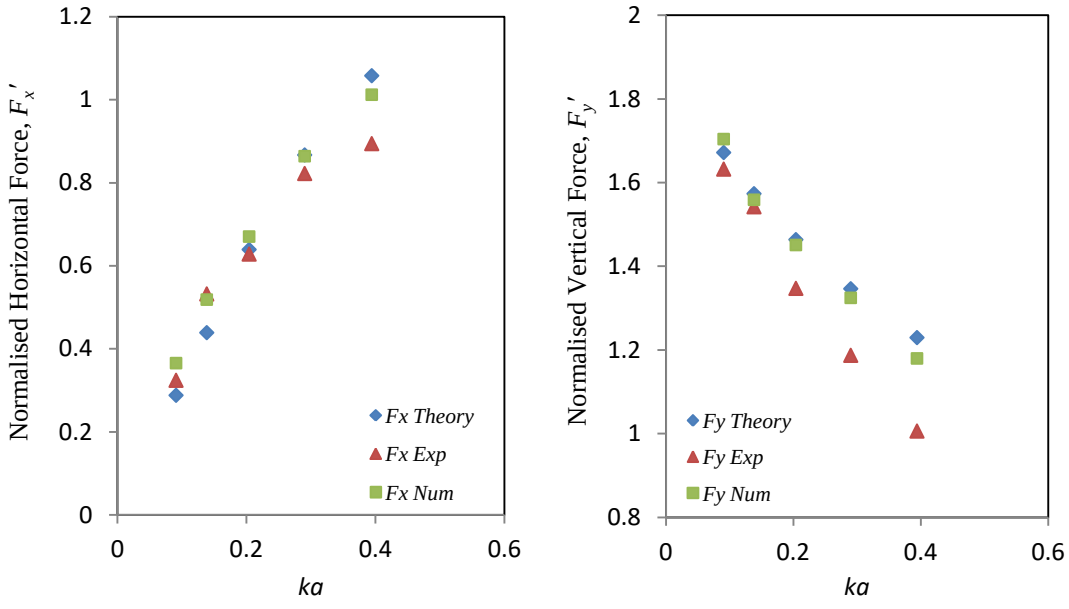

(a) F_x' (b) F_y'

Fig. 7(a)-(b): Comparison of normalised F_x' and F_y' forces between numerical results, potential theory and experimental data by Martin and Dixon (1983) for test cases (7-11) in terms of ka.

3.3 Validations for forces with Morison equation and experimental data

The numerical horizontal and vertical forces produced in this section are based on some of the test cases presented in Table 2 in Section 3.1. The cylinder is subject to incident waves of various wave amplitudes with a constant frequency of 1 Hz and a wavelength of 1.539 m. Fig. 8(a) - (e) show the comparisons between the typical non-dimensionless horizontal forces of the numerical results, experimental data (Dixon et al. 1979 and Dixon, 1980) and the Morison equation theoretical prediction discussed in Section 2.4 for a selection of relative wave amplitudes, A'. Fig. 9(a) - (e) show the equivalent comparisons for the vertical forces. In Figures 8(a) - 8(e), the Morison equation shows the same overall trend with the numerical results. However, the Morison equation shows increasing deviation from the numerical results with increasing wave amplitude. Experimental data also shows the same overall trend agreement with the numerical results and the Morison equation. It is noted that numerical results appear to show better agreement with experimental data for larger wave amplitudes.

In Fig. 9(a) and 9(b), the typical vertical forces over one time period show a good sinusoidal behaviour, as expected since the data ($A/a \leq 0.4$) is within the linearised wave theory range. There is reasonable agreement between numerical results, experimental data and the theoretical vertical forces in Fig. 9(a) and (b). For larger wave amplitudes considered in Fig. 9(c) - (e), the numerical results show a non-sinusoidal behaviour which is consistent with the trend in the experimental data. However, in these figures the Morison equation shows some discrepancy with both numerical results and experimental data. This discrepancy is to be expected since the Morison empirical equation is based on a number of simplifying assumptions but is consistent with the numerical results and experimental data in terms of non-linear behaviour. Fig. 10(a) - (j) show the wave elevation around the cylinder over one time period for test case 6 ($A' = 0.5$) in Fig. 9(e). The numerical result gives reasonable prediction for the experimental data on the non-linear behaviour of the vertical force in Fig. 9 (e). The non-linear behaviour is likely due to the combined effects of the weight of the water during overtopping in Fig. 10(d) and restored buoyancy after the wave has passed as seen in Fig. 10(h). This behaviour is consistent with the findings of Andersson (2011), Westphalen et al. (2012), and Bihs and Ong (2013) for the large wave amplitude ($A' = 0.5$).

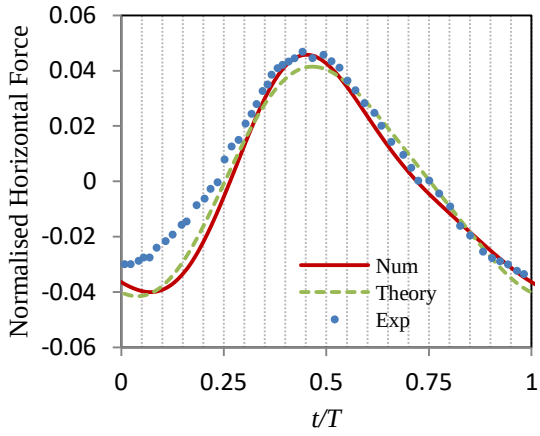

(a) $A' = 0.1$

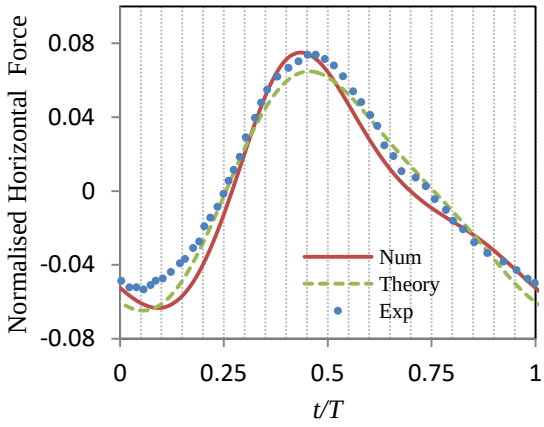

(b) $A' = 0.15$

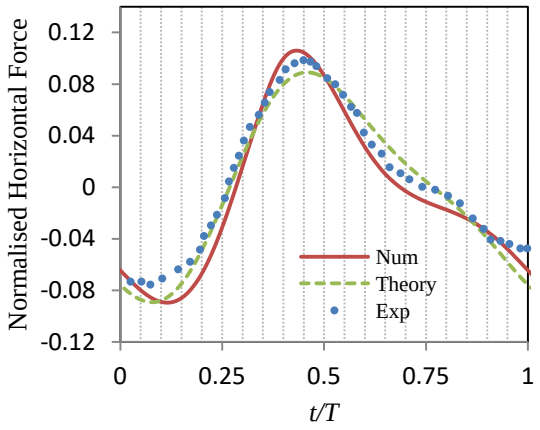

(c) $A' = 0.2$

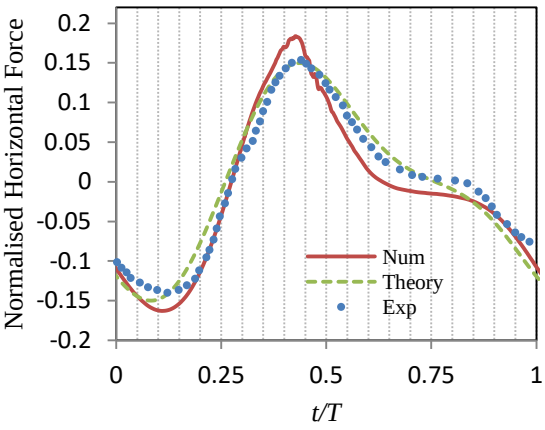

(d) $A' = 0.3$

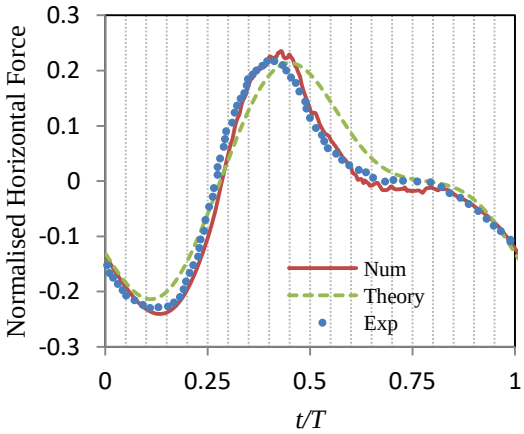

(e) $A' = 0.4$

Fig. 8(a) - (e): Comparison of normalised numerical, experimental and theoretical (Morison equation) horizontal force for some of the test cases in Table 2.

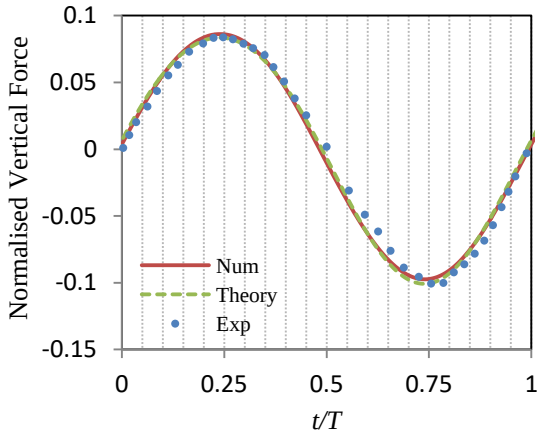

(a) $A' = 0.1$

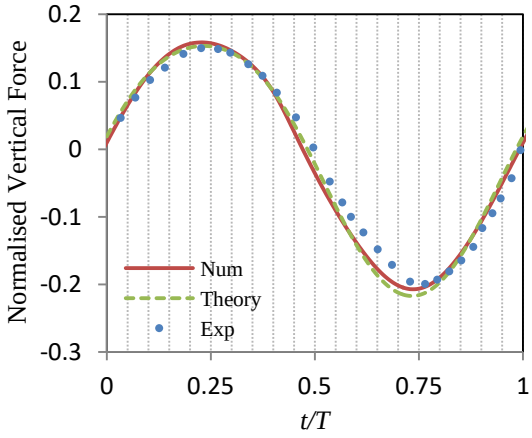

(b) $A' = 0.2$

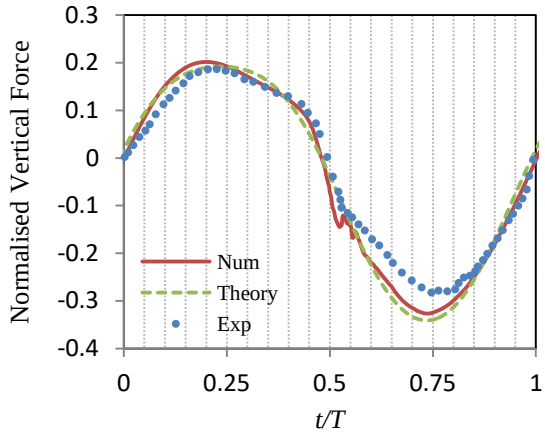

(c) $A' = 0.3$

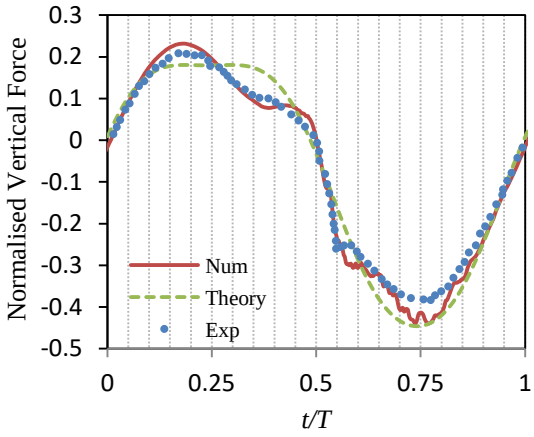

(d) $A' = 0.4$

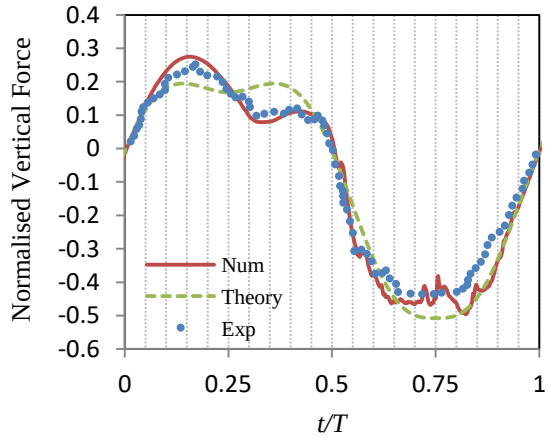

(e) $A' = 0.5$

Fig. 9(a) - (e): Comparison of normalised numerical, experimental and theoretical (Morison equation) vertical force for some of the test cases in Table 2.

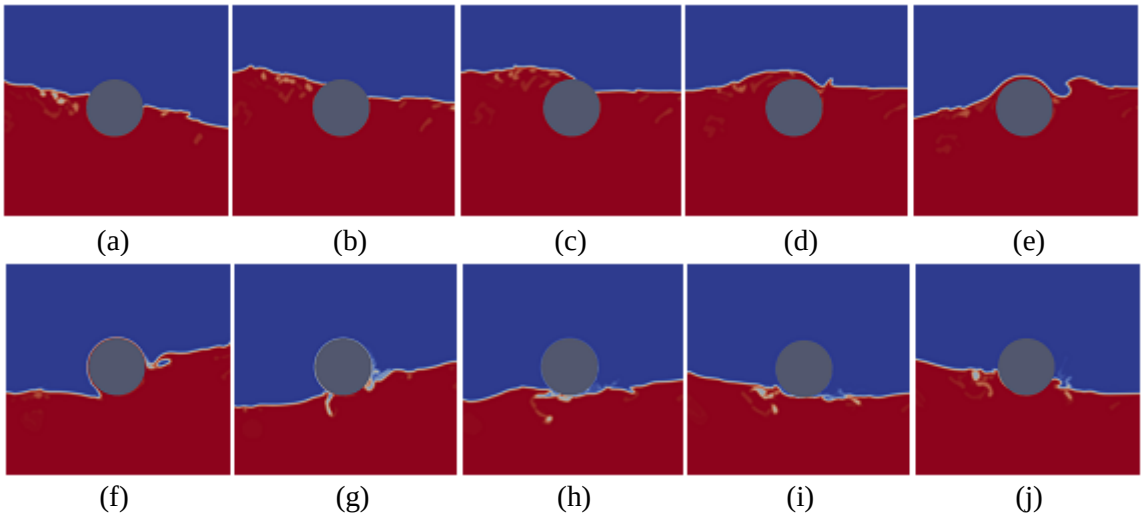

Fig. 10(a) - (j) Screenshots of wave elevation around the cylinder over one time period (one cycle) at (a) t/T = 0.05, (b) t/T = 0.15, (c) t/T = 0.25, (d) t/T = 0.35, (e) t/T = 0.45, (f) t/T = 0.55, (g) t/T = 0.65, (h) t/T = 0.75, (i) t/T = 0.85, (j) t/T = 0.95 for test case 6, A' = 0.5.

3.4 Computational domain setup for a vertically oscillating horizontal cylinder

The simulations of a vertically oscillating semi-immersed horizontal cylinder are conducted in a 30 m long NWT as shown in Fig. 11(a). The test cases are developed for two cylinders radii of 0.076 m and 0.152 m, for the semi-circular section below the water line. Above the water line the section is considered as a rectangular section with vertical sides being extended 0.102 m above the mean free surface. The rectangular section above the water line is chosen to be consistent with the experimental setup used by Yu and Ursell (1961). Both cylinders are immersed in a NWT with different water depths of 0.267 m and 0.577 m, where the cylinder axis is located at the centre of the NWT on the free surface. Fig. 11(a) shows the schematic of the computational domain setup for the NWT and Fig. 11(b) shows the close up of the two cylinder dimensions.

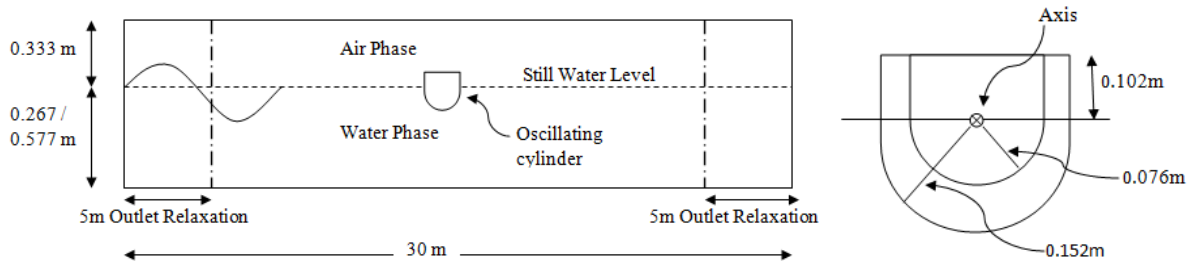

(a) NWT setup (b) close-up of cylinders

Fig. 11(a) - (b): Schematic of the computational domain setup for the oscillating cylinder in the NWT (not drawn to scale).

The water depth to cylinder radius ratio, h/a, for the four new simulation test cases (1 - 4) are chosen to be 1.75, 3.50, 3.79 and 7.58 respectively as shown in Table 4. Measurements are

taken for each of the four ratios with different amplitudes of the cylinder displacement, α and wave periods, $T = \sqrt{(2\pi L_\infty)/g}$, where L_∞ is the wavelength associated with an infinite water depth defined by Yu and Ursell (1961). Based on the experimental evidence by Yu and Ursell (1969), values of $2\pi a/L_\infty$ are to be restricted to less than 3.0, since water in the gaps between the side walls of the channel and the ends of the cylinder tended to oscillate violently at higher frequencies.

Table 4: Parameters for the simulation

Test Case	***a*, radius (m)**	***h*, water depth (m)**	***h/a*, ratio**
1	0.152	0.267	1.75
2	0.076	0.267	3.5
3	0.152	0.577	3.79
4	0.076	0.577	7.58

To model the free surface waves in the NWT, the simulations are set up similarly as in the simulations discussed in Section 3.1. For example, the time scheme and time step function; boundary condition of the horizontal top, cylinder wall and tank bed floor; air and water density and kinematic viscosity are all set to be the same as in Section 3.1. The different settings are application of a no-slip boundary condition on both outlet boundaries and two 5 m outlet relaxation zones near both ends of the NWT. Since the simulations involve oscillating movement of a cylinder, the cylinder boundary is set to 'patch' in the dynamic mesh dictionary in OpenFOAM® to allow mesh motion in the vertical direction. The oscillating displacement function under the 'fvMotionSolver' library in OpenFOAM®, is used for prescribing the required displacement amplitude, α, where a pre-defined sequence of mesh changes is made to accommodate the motion. The interDyMFoam solver, which consists of dynamic mesh functionality, is coupled with the waves2Foam libraries for running the simulations. An unstructured mesh for the computational domain is constructed for each of the test cases (1 - 4) in Table 4 using blockMesh and snappyHexMesh. The mesh is refined along the free surface area and around the cylinder as shown in Fig. 12. The refinement region closest to the free-surface and cylinder has a grid size of 0.3 cm x 0.3 cm. Since measurements of the surface elevation are shown to be identical on both ends of the NWT (left and right sides from the cylinder axis) for test case 1, the number of mesh elements on one end of the NWT (not used for taking measurements) for the remaining test cases is reduced significantly to improve computational efficiency. A symmetry plane can also be considered in the future to further improve the computational efficiency.

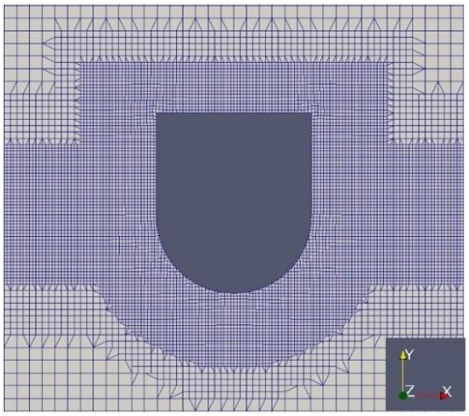

Fig. 12: Close up of the mesh around the cylinder for test case 1.

According to Yu and Ursell (1969), the wave absorbers were not able to absorb the waves completely in the physical experiment. The experiments were purposely run for a long period of time before any measurements were taken to allow wave reflections to take place. The measured maximum and minimum wave height were then taken by moving the position of the wave gauge slowly towards the cylinder in the experiment. These measurements are required to determine the amplitude reflection coefficient, in which corrections are then carried out to ensure the wave amplitudes predictions are based on an infinite tank length. The reflection coefficient correction is not taken into account in the simulations since the wave relaxation zones are capable of preventing wave reflections. For all the numerical measurements, a fixed probe is located at a horizontal distance of 2 m from the axis of the cylinder to capture the surface elevation as a function of time. Fig. 13 shows a screenshot of the NWT, where surface waves are generated during the simulation for a typical test case.

Fig. 13: Screenshot of the oscillating cylinder in the NWT during simulation. Volume fraction (alpha1) field, where 0 = air and 1 = water.

3.5 Validations on amplitude ratio of surface waves

The numerical simulations for each of the four test cases are run for a 20 second period. The amplitude of the surface wave is evaluated when the wave elevations have reached a steady-state (a ramp function is included for the oscillations to occur gradually to prevent rapid transient waves). The amplitude ratio R_A is defined as the amplitude of the surface wave divided by the displacement amplitude of the cylinder, α. The amplitude ratio, R_A, was plotted against $2\pi a/L_\infty$ in Fig. 14(a) - (d), where comparisons are made between the theoretical predictions, experimental data and numerical results for test cases (1 - 4) respectively. In all test cases, the numerical amplitude ratios, R_A shows reasonable agreement with both Yu and

Ursell's (1969) theoretical predictions and experimental data. The numerical results for all test cases show particularly good agreement with theory at low values of $2\pi a/L_\infty$ but show some discrepancies at higher values of $2\pi a/L_\infty$. This discrepancy is likely to be due to non-linear effects since the numerical results are outside of the linear wave theory region.

With regard to the comparison between numerical results and experimental data shown in Fig. 14(a) - (d), the numerical results are usually within ± 5% of the experimental data for test case 1 and 2, whilst the numerical results are usually within ± 3% of the experimental data for test case 3 and 4. The numerical prediction generally lies within the error bars of the experiment, and follows the trend observed in the experiment in the non-linear region. The discrepancy between numerical and experimental data could be due to the resolution of the instrumentation used to produce the experimental data especially on measuring small wave amplitudes. According to Yu and Ursell (1969), a maximum error of 3% was stated for the accuracy of the experimental measurements. Another possible explanation for the overall discrepancy between the numerical resutls and the experimental data is that wave reflections took place in the experiment as mentioned in Section 3.4. In the numerical simulation, relaxation zones are set up to absorb the waves near the outlet boundaries and to eliminate reflections. In addition, the difference between the three-dimensional (3D) experiment and the 2D simulation may partially explain the deviations between the numerical results and the experimental data. All the measurement details of the numerical results, experimental data and theoretical predictions produced in this study are presented in Table A1 - A4 in Appendix I.

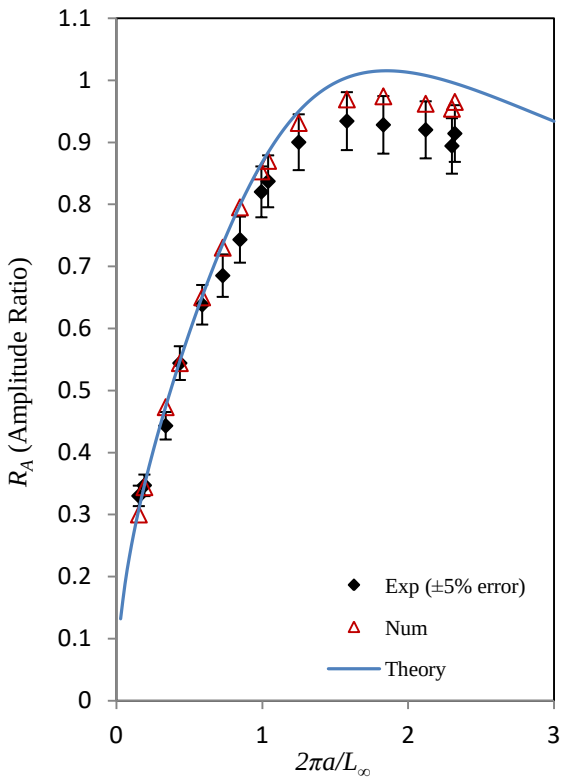

Fig. 14(a): Test Case 1 (h/a =1.75)

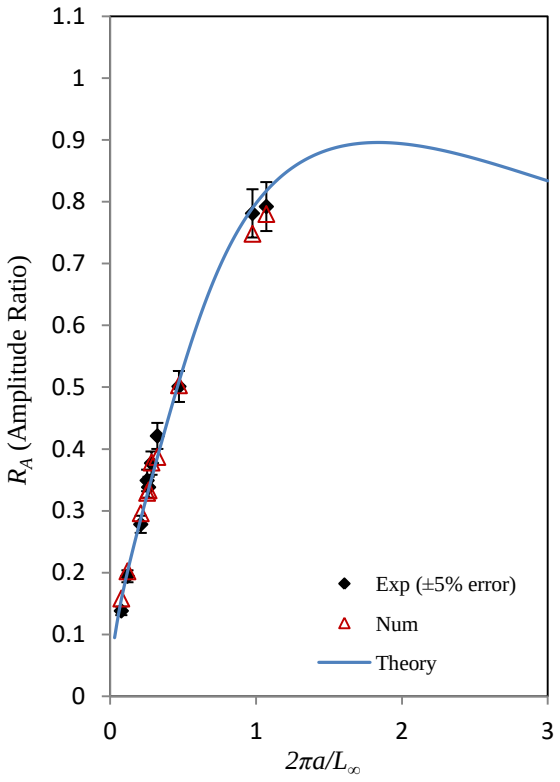

Fig. 14(b): Test Case 2 (h/a =3.5)

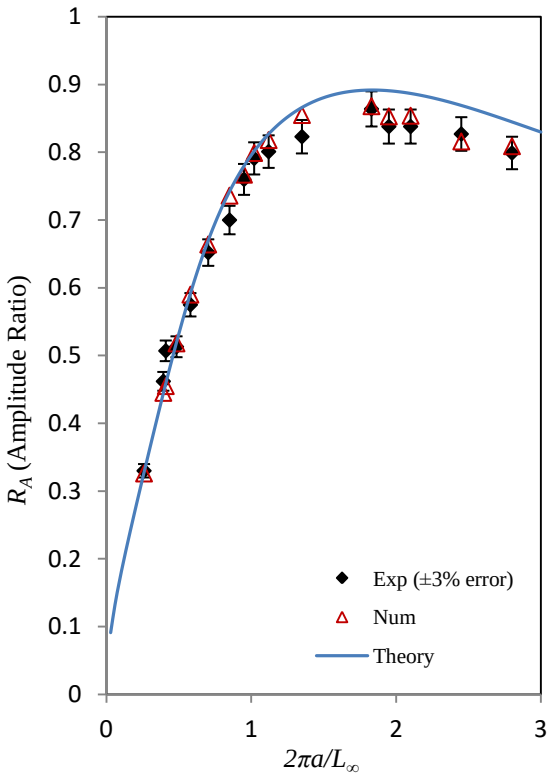

Fig. 14(c): Test Case 3 (h/a =3.79)

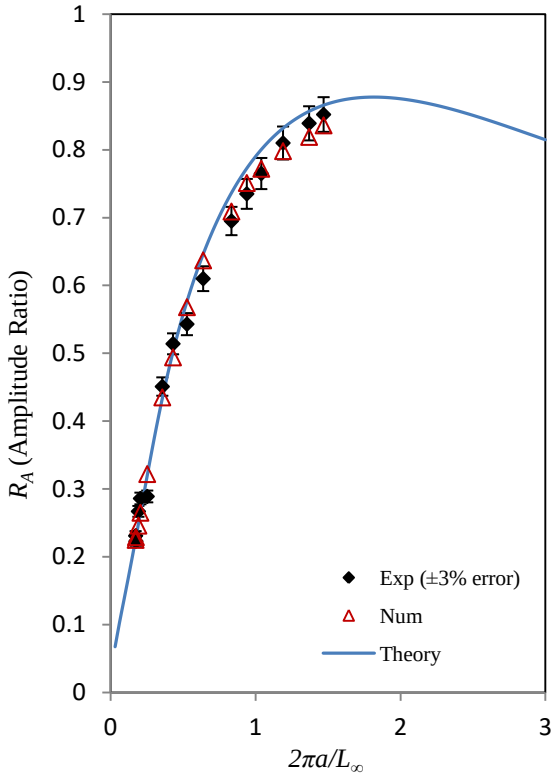

Fig. 14(d): Test Case 4 (h/a =7.58)

4. Conclusions

This paper provides a valuable contribution in revisiting classic fluid-structure interaction benchmark cases, such as a fixed and a vertically oscillating semi-immersed horizontal cylinder, with a more thorough investigation using a fully non-linear CFD approach that provides genuine insight in to how reliable OpenFOAM® predicts the details of non-linearities, as well as showing the validity and the limitation of the linear and non-linear theory. Of particular interest in the paper are the horizontal and vertical force calculations acting on the fixed semi-immersed horizontal cylinder due to wave interactions in a 2D NWT. Numerical predictions are compared with linear theories which take into account wave diffraction and a non-linear theory based on a semi-empirical method. The surface waves generated by the motion of the oscillating cylinder are computed in which the amplitude ratio is compared with theoretical predictions based on potential flow theory. Both studies are also compared with available experimental data in the literature.

The OpenFOAM® software package and waves2Foam toolbox are capable of accurately predicting wave characteristics in a 2D NWT and have the ability to capture the non-linear effects of fluid-structure interactions for a wide range of wave and body motion regimes. Suitable length relaxation zones placed at the NWT are shown to absorb satisfactorily wave reflections from both inlet and outlet boundaries.

The numerical wave force predictions acting on a fixed semi-immersed horizontal cylinder give broad overall agreement with approaches based on the linear wave theory and available experimental data, under small wave amplitude conditions ($A/a \leq 0.4$). Some discrepancy occurs between theory and numerical wave force data for larger wave amplitudes, as expected, since the numerical results are outside the range of the linear wave theory. For large amplitude waves, the numerical force non-linearities are consistent with the trend in the experimental data and the Morison equation theory. The variation of numerical wave force data with wave frequency also shows good agreement with theory and experimental data at low frequencies ($ka < 0.2$). Comparison of numerical force data with available experiment data show some deviations at higher wave frequencies which are likely to be due to the differences in the wave generation and wave absorption methods used in the NWT and the physical wave tank. A vertically oscillating semi-immersed horizontal cylinder in a NWT produced wave amplitude ratios which are in good agreement with approaches based on linear theory and experimental data for long wavelengths. However for shorter wavelengths, the theory differs slightly from the numerical data which is likely due to the non-linear wave effects. The overall agreement between the numerical wave amplitudes and experimental data is within ±5% for the wavelengths considered in the simulations.

The presented results in this study indicate that the numerical predictions are consistent with the experimental data, approaches based on the linearised wave theory and the Morison equation considered in the literature. It has been demonstrated in this paper that the CFD model is able to provide a comprehensive understanding of the hydrodynamic analysis of wave-structure interactions on a semi-immersed horizontal cylinder, as well as to give useful guidance and confidence to WEC developers especially on the design considerations relevant

to the WEC systems. The application of CFD modelling is therefore a practical approach that may be used for predicting complex wave-structure interactions in WECs. Further improvement such as simulating a full 3D model under turbulent flow can be considered to capture the 3D effects and the non-linear effects more accurately. Incorporating the physical behaviour of a dynamic wave paddle in the lab numerically might provide a closer representation of the wave generation method in a NWT instead of imposing an incoming velocity field in the inlet boundary.

Acknowledgement

This research is partly funded by the School of Marine Science and Engineering at Plymouth University and was carried out as part of an industrial PhD collaboration project formerly associated with Pelamis Wave Power.

Appendix I

Table A1: Parameters and measurements for test case 1 (a, radius = 0.152 m and h, water depth = 0.267 m, h/a = 1.75).

Run no.	L_∞ (m)	ω (rad/s)	2α (m)	$2\pi a/L_\infty$	R_A Experiment	R_A Theory	R_A Numerical = Amp/α	% Error (Num vs Exp)	% Error (Num vs Theory)
1	6.248	3.141	0.0324	0.154	0.33	0.307	0.300	-9.091	-2.280
2	5.000	3.511	0.0324	0.192	0.347	0.346	0.344	-0.865	-0.578
3	2.838	4.660	0.0324	0.338	0.443	0.473	0.473	6.772	0.000
4	2.204	5.288	0.0263	0.435	0.544	0.542	0.544	0.000	0.369
5	1.631	6.147	0.0263	0.588	0.638	0.65	0.65	1.881	0.000
6	1.314	6.849	0.0263	0.729	0.685	0.736	0.73	6.569	-0.815
7	1.131	7.382	0.0263	0.847	0.743	0.798	0.795	6.999	-0.376
8	0.963	8.000	0.0183	0.994	0.82	0.865	0.853	4.024	-1.387
9	0.920	8.185	0.0263	1.04	0.837	0.883	0.87	3.943	-1.472
10	0.768	8.959	0.0131	1.25	0.9	0.949	0.931	3.444	-1.897
11	0.607	10.077	0.0191	1.58	0.934	1.004	0.969	3.747	-3.486
12	0.524	10.846	0.0192	1.83	0.928	1.015	0.974	4.957	-4.039
13	0.451	11.691	0.0143	2.12	0.92	1.008	0.962	4.565	-4.563
14	0.418	12.143	0.0143	2.3	0.894	0.997	0.954	6.711	-4.313
15	0.415	12.187	0.0143	2.32	0.914	0.996	0.965	5.580	-3.112

Table A2: Parameters and measurements for test case 2 (a, radius = 0.076 m and h, water depth = 0.267 m, h/a = 3.5).

Run no.	L_∞ (m)	ω (rad/s)	2α (m)	$2\pi a/L_\infty$	R_A Experiment	R_A Theory	R_A Numerical =Amp/α	% Error (Num vs Exp)	% Error (Num vs Theory)
1	2.01	3.126	0.0324	0.076	0.138	0.156	0.158	14.493	1.282
2	1.611	3.9	0.0324	0.118	0.194	0.201	0.202	4.124	0.498
3	1.19	5.28	0.0324	0.209	0.278	0.293	0.296	6.475	1.024
4	1.1	5.712	0.0324	0.253	0.349	0.326	0.329	-5.731	0.920
5	1.081	5.812	0.023	0.263	0.338	0.334	0.333	-1.479	-0.299
6	0.994	6.321	0.0324	0.283	0.377	0.375	0.378	0.265	0.800
7	0.974	6.451	0.023	0.323	0.421	0.386	0.387	-8.076	0.259
8	0.806	7.796	0.023	0.471	0.501	0.509	0.503	0.399	-1.179
9	0.561	11.2	0.0238	0.975	0.781	0.79	0.748	-4.225	-5.316
10	0.534	11.766	0.0238	1.07	0.792	0.819	0.78	-1.515	-4.762

Table A3: Parameters and measurements for test case 3 (a, radius = 0.152 m and h, water depth = 0.577 m, h/a = 3.79).

Run no.	L_∞ **(m)**	ω **(rad/s)**	2α **(m)**	$2\pi a/L_\infty$	R_A **Experiment**	R_A **Theory**	R_A **Numerical =Amp/**α	**% Error (Num vs Exp)**	**% Error (Num vs Theory)**
1	3.688	4.088	0.0268	0.26	0.33	0.327	0.326	-1.212	-0.306
2	2.438	5.028	0.0266	0.393	0.462	0.444	0.445	-3.680	0.225
3	2.338	5.135	0.0265	0.41	0.507	0.458	0.455	-10.256	-0.655
4	1.978	5.582	0.0266	0.484	0.513	0.519	0.518	0.975	-0.193
5	1.652	6.108	0.0266	0.58	0.575	0.591	0.59	2.609	-0.169
6	1.363	6.725	0.0266	0.703	0.652	0.67	0.664	1.840	-0.896
7	1.128	7.392	0.0266	0.85	0.70	0.742	0.736	5.143	-0.809
8	1.009	7.816	0.0267	0.95	0.76	0.78	0.767	0.921	-1.667
9	0.939	8.102	0.0131	1.02	0.791	0.802	0.799	1.011	-0.374
10	0.853	8.501	0.0131	1.12	0.801	0.828	0.818	2.122	-1.208
11	0.71	9.317	0.0185	1.35	0.823	0.866	0.855	3.888	-1.270
12	0.524	10.846	0.0141	1.83	0.864	0.892	0.868	0.463	-2.691
13	0.494	11.17	0.0197	1.95	0.838	0.891	0.853	1.790	-4.265
14	0.457	11.614	0.014	2.1	0.838	0.887	0.854	1.909	-3.720
15	0.39	12.572	0.0206	2.45	0.827	0.869	0.816	-1.330	-6.099
16	0.341	13.444	0.0206	2.8	0.799	0.845	0.809	1.252	-4.260

Table A4: Parameters and measurements for test case 4 (a, radius = 0.076 m and h, water depth = 0.577 m, h/a = 7.58).

Run no.	L_∞ **(m)**	ω **(rad/s)**	2α **(m)**	$2\pi a/L_\infty$	R_A **Experiment**	R_A **Theory**	R_A **Numerical =Amp/**α	**% Error (Num vs Exp)**	**% Error (Num vs Theory)**
1	2.774	4.714	0.0303	0.173	0.231	0.227	0.225	-2.597	-0.881
2	2.743	4.74	0.0303	0.175	0.223	0.23	0.229	2.691	-0.435
3	2.499	4.966	0.0303	0.192	0.267	0.249	0.246	-7.865	-1.205
4	2.32	5.154	0.0303	0.206	0.286	0.267	0.265	-7.343	-0.749
5	1.89	5.711	0.0303	0.253	0.289	0.322	0.322	11.419	0.000
6	1.341	6.78	0.0246	0.357	0.451	0.435	0.435	-3.548	0.000
7	1.113	7.442	0.0246	0.431	0.514	0.503	0.494	-3.891	-1.789
8	0.908	8.239	0.0246	0.527	0.543	0.577	0.568	4.604	-1.560
9	0.75	9.066	0.0246	0.639	0.61	0.647	0.637	4.426	-1.546
10	0.57	10.4	0.0246	0.834	0.695	0.739	0.709	2.014	-4.060
11	0.509	11.004	0.0215	0.94	0.735	0.773	0.751	2.177	-2.846
12	0.46	11.576	0.0156	1.04	0.765	0.801	0.772	0.915	-3.620
13	0.402	12.383	0.0182	1.19	0.81	0.832	0.798	-1.481	-4.087
14	0.351	13.252	0.0167	1.37	0.839	0.856	0.819	-2.384	-4.322
15	0.326	13.75	0.0186	1.47	0.852	0.866	0.836	-1.878	-3.464

References

Andersson, J., (2011). “Simulation of Wave Induced Forces on Semi Submerged Horizontal Cylinders Using OpenFOAM®”, Master of Science Thesis in the Master Degree Programme Naval Architecture, Department of Shipping and Marine Technology, Chalmers University of Technology, Sweden.

Bihs, H., Ong, M.C., (2013). “Numerical simulation of flows past partially-submerged horizontal circular cylinders in free surface waves”, In: Proceedings of the ASME 2013 32nd International Conference on Ocean, Offshore and Arctic Engineering, OMAE2013-10529, June 9–14, Nantes, France.

Borgman, L.E., (1958). “Computation of the Ocean Forces on an Infinitely Long Circular Cylinder in an Oblique Sea”, Transactions of the American Geophysical Union, Vol 39, no 5, pp 885-888.

Chakrabarti, S.K., Tam W.A., Walbert A.L., (1975). “Wave Forces on a Randomly Oriented Tube”, presented at the May 5-8 Seventh Annual Offshore Technology Conference, Houston, Texas (Paper OTC 2190).

Chen, B., Lu, L., Greated C.A., Kang, H., (2015). “Investigation of wave forces on partially submerged horizontal cylinders by numerical simulation”, Ocean Engineering, 107, pp. 23–31.

Chung M.-H., (2015). “Hydrodynamics of flow over a transversely oscillating circular cylinder beneath a free surface”, Journal of Fluids and Structures, Vol. 54, 27-73.

Dean, R.G., Ursell, F., (1959). “Interaction of a fixed, semi-immersed circular cylinder with a train of surface waves”, Tech. Rep. No. 36. Hydro. Lab, Massachusetts Inst. of Tech.

Dixon, A.G., Greated, C.A., Salter, S.H., (1979). “Wave Forces on Partially Submerged Cylinders”, Journal of the Waterway Port Coastal and Engineering Division, Nov, no WW4, pp 421-437.

Dixon, A.G., (1980). “Wave Forces on Cylinders”, Doctoral Thesis. University of Edinburgh, Edinburgh.

Frank, W., (1967). “Oscillation of cylinders in or below the free-surface of deep fluids”, Technical Report 2375, Naval Ship Research and Development Centre, Washington D.C., USA.

Fuhrman, D.R., Madsen, P.A., Bingham, H.B., (2006). “Numerical simulation of lowest order short-crested wave instabilities”, J. Fluid Mech. Vol. 563, 415–441.

Gadelho, A. L. J., Rodrigues, J. M., Soares, C. G., (2014). “Determining hydrodynamic coefficients of a cylinder with Navier-Stokes equations”, Maritime Technology and Engineering, 1001-1007.

Garrison, C.J., Rao, V.S., (1971). “Interaction of Waves with Submerged Objects”, Journal of the waterways, Harbors and Coastal Engineers Division, ASCE, Vol.97, no WW2, Proc. Paper 8111, pp 259-277.

Greenshields, C., (2015). “OpenFOAM®: User Guide Version 2.4.0”, Available from http://foam.sourceforge.net/docs/Guides-a4/UserGuide.pdf. Last accessed 10th September 2015.

Hirt, C.W., Nichols, B.D., (1981). “Volume of Fluid (VOF) Method for the Dynamics of Free Boundaries”, Journal of Computational Physics 39, 201, 1981.

Jacobsen, N. G., Fuhrman, D. R., Fredøe, J., (2012). “A wave generation toolbox for the open-source CFD library: OpenFOAM®”, International Journal for Numerical Methods in Fluids, 70, 1073-1088.

Le Méhauté, B., (1976). “An introduction to hydrodynamics and water waves”, Springer, ISBN 0-387-07232-2.

Martin, P. A., Dixon, A. G., (1983). “The Scattering of regular surface waves by a fixed, half-immersed, circular cylinder”, Applied Ocean Research, 1983, Vol. 5, No 1.

Mayer, S., Garapon, A., Sørensen, L.S., (1998). “A fractional step method for unsteady freesurface flow with applications to non-linear wave dynamics”, Int. J. Numer. Methods Fluids 28 (2), 293–315.

Morison, J.R., O'Brien, M.P., Johnson, R.W., Schaaf, S.A., (1950). “The Force Exerted by Surface Waves on Piles”. Petroleum Transaction, American Institute of Mining, Metallurgical and Petroleum Engineers, Vol. 189, pp. 149-154.

Ong, M. C., Kamath, A., Bihs, H., Afzal, M. S., (2017). “Numerical simulation of free-surface waves past two semi-submerged horizontal circular cylinders in tandem”, Marine Structures, 52, 1-14.

Ramos, J., Guedes Soares, C., (1997). “On the Assessment of Hydrodynamic Coefficients of Cylinders in Heaving”, Ocean Engineering; 24(8), pp.743–763.

Sutulo, S., Rodrigues, J.M., Guedes Soares C., (2009). “Computation of inertial and damping characteristics of ship sections in shallow water”, Ocean Engineering. Vol. 36, pp. 1098-1111.

Sutulo, S., Rodrigues, J. M., Guedes Soares, C. (2010). “Hydrodynamic characteristics of ship sections in shallow water with complex bottom geometry”, Ocean Engineering, Vol. 37, pp. 947-958.

Tasai, F., (1960). “Formula for calculating hydrodynamic force on a cylinder heaving in the free surface, (N-Parameter Family)”, Technical Report Vol. VIII, No 31. Research Institute for Applied Mechanics, Kyushu University, Japan.

Tasai, F., (1961). “Hydrodynamic force and moment produced by swaying and rolling oscillation of cylinders on the free surface”, Technical Report Vol. IX, No 35. Research Institute for Applied Mechanics, Kyushu University, Japan.

Thorne, R. C., (1953). “Multipole expansion in the theory of surface waves”, Proc. Camb. Phil. Soc. 49, 707-716.

Ursell, F., (1949). “On the heaving motion of a circular cylinder in the surface of a fluid”, quart. J. Mech. Appl. Math. 2, pp. 218–231.

Vugts, J.H., (1968). “The hydrodynamic coefficients for swaying, heaving and rolling cylinders on a free surface”, Shipbuilding Laboratory, Technical Uniersity of Delft.

Westphalen, J., Greaves, D.M., Williams, C.J.K, Hunt-Raby, A.C., Zang, J. (2012). “Focused waves and wave-structure interaction in a numerical wave tank”, Ocean Engineering, Vol. 45, pp. 9–21.

Yu, Y.S., Ursell, F. (1961). “Surface waves generated by an oscillating circular cylinder on water of finite depth: theory and experiment”, J. Fluid Mech., Vol. 11, pp. 529-551.